Carbon 204 (2023) 254–267

Contents lists available at ScienceDirect

Carbon

journal homepage: www.elsevier.com/locate/carbon

Thiol functionalized activated carbon for gold thiosulfate recovery, an analysis of the interactions between gold and sulfur functions

Nathalie de la Torre-Miranda, Laoise Reilly, Pierre Eloy, Claude Poleunis, Sophie Hermans *

Université Catholique de Louvain, Institut de La Matière Condensée et des Nanosciences (IMCN), Place Louis Pasteur 1, B-1348, Louvain-la-Neuve, Belgium

ARTICLE INFO

Keywords:
Gold thiosulfate
Activated carbon functionalization
Thiol functions
Adsorption
Mechanism
Elution

ABSTRACT

Cyanide salts are currently used as leaching agents in gold extraction processes despite their toxicity. Thiosulfate is a greener choice, but its employment is constrained by the difficulty at recovering gold thiosulfate from the leachate using activated carbon, which in contrast, works well for gold-cyanide adsorption. Aiming to solve this problem, activated carbon has been covalently functionalized with thiol groups (-SH) through a peptide bond formation with cysteamine, as thiol-carrier molecule. The functionalized carbon accomplishes up to 100% Au recovery (with 2 and 25 ppm Au solution) in 8 h contact and its performance seems independent on the solution's pH. In-depth solid characterization techniques (XPS, TOF-SIMS, FTIR, PXRD, TEM, N_2 physisorption, elemental analysis) have been used to unravel the interactions between Au thiosulfate and thiol functions and two different gold adsorption mechanisms have been demonstrated: under acid conditions, the formation of Au^{1+}- S chains has been proven. Under basic conditions, Au^0 species have been detected in addition to Au^{1+}- S chains. Elution of the gold loaded samples has been accomplished at a 71% level using $Na_2S_2O_3$ and NH_4OH as eluents.

1. Introduction

Gold mining is a relevant productive activity with operations on all the continents, except Antarctica. In 2020, more than 3400 metric tons of gold were exploited from mines at different scales, from which 15–20% are considered as artisanal and small-scale mining production (ASM) [1,2]. In ASM, gold extractive processes like mercury amalgamation and cyanidation are vastly employed due to their technical simplicity and low cost [3]. Currently, more than 70 countries in Africa, Latin America and Asia use these recovery procedures despite their environmental and health impacts [4,5].

Since its invention in the 1800s, cyanidation was proposed as a more efficient alternative to ancestral amalgamation practices to recover fine gold (<0.2 mm particle size) [4]. In this process, a cyanide salt (NaCN or KCN) is added to leach gold from the previously ground mineral (10–20% solids). Then, either Merrill-Crow (cementation of gold using Zn powders [6]) or Carbon-in-Pulp (sorption of gold cyanide onto granular activated carbon [7]) processes are implemented to recover the gold-cyanide complex from the leaching solution [4]. Even though cyanidation has been proven efficient, simple and cost-effective, it is impossible to deny the health risk that its handling represents. Furthermore, the lack of clean mining practices and adequate tailing treatment that are constantly seen in ASM have caused irreversible pollution in rivers and soils and everlasting damage [3,8].

For these reasons, aiming at finding greener and sustainable alternatives, research in gold recovery is nowadays focusing on proposing non-pollutant gold lixiviants. Among those, thiosulfate is considered as a suitable option due to its low toxicity (its complexes are currently used as fertilizer and potential antidote to cyanide and arsenic), high gold leaching efficiency and low cost [9–11]. Thiosulfate $S_2O_3^{2-}$ achieves to dissolve gold from the ore in alkaline solutions in the presence of an oxidant like oxygen, forming the stable, anionic complex $[Au(S_2O_3)_2]^{3-}$ according to the following main reaction [9]:

$$4\ Au + 8\ S_2O_3^{2-} + O_2 + 2H_2O \rightarrow 4\ [Au(S_2O_3)_2]^{3-} + 4\ OH^-$$

However, one of the main drawbacks of this method is the difficulty to recover $[Au(S_2O_3)_2]^{3-}$ from the leaching solution, as it has low affinity for cheap sorbents like granular activated carbon, that in contrast, can easily trap gold-cyanide complexes [9,12]. An alternative for $[Au(S_2O_3)_2]^{3-}$ recovery is strong base resins, consisting mainly of amines attached to a polymer backbone. Nevertheless, their main disadvantages are their low mechanical resistance to abrasion, making it difficult to work in contact with mineral pulps, their small particle sizes that require fine filters and costly centrifugation methods and their sensibility to

* Corresponding author.
E-mail address: sophie.hermans@uclouvain.be (S. Hermans).

https://doi.org/10.1016/j.carbon.2022.12.061
Received 13 October 2022; Received in revised form 8 December 2022; Accepted 20 December 2022
Available online 21 December 2022
0008-6223/© 2022 Elsevier Ltd. All rights reserved.

osmotic shock [13]. In consequence, the industrial use of thiosulfate is rare nowadays, limiting its application to minerals with preg-robbing carbon [9,10].

Activated carbon (AC) is a complex, graphitic-type carbon with extensive internal porosity and great surface area (up to 1500 m^2/g) [14,15]. It is used in a variety of applications due to its high adsorption capacity of organic and inorganic compounds, whose affinity is determined by both its physical structure (porosity) and chemical components [15,16]. Furthermore, the presence of heteroatoms like oxygen, sulfur and nitrogen, that could be derived from the raw material or added by specific preparation or post-treatments procedures, are the key for its chemical reactivity and adsorption capacity [17]. Indeed, activated carbon could be intentionally modified by different techniques to enrich it with a specific heteroatom that would increase the adsorption capacity for a desired compound. In this context, sulfur containing functional groups, specifically thiols (-SH), represent an attractive functionalization option, since their affinity for gold is well-known and they could be grafted in activated carbons with simple functionalization processes [18,19].

Grafting thiol groups onto carbon materials has been carried out for several purposes before. These carbons have been employed in, for example, transition metal nanoparticles anchoring [18,20], immobilization of nanotubes onto gold tips for scanning tunneling microscopy imaging [21], preparation of ordered and aligned nanotubes on gold surfaces [22], *etc*. Regarding metallurgical applications, Yunlong Chen et al. [23,24] have worked on activated carbon modification with aromatic nitrogen and sulfur-containing molecules through non-covalent functionalization methods for gold thiosulfate recovery. Since their choice has been non-covalent functionalization, the only elution alternative proposed has been washing the gold loaded solid with organic solvents, which are toxic and difficult to be handled at industrial-scale level. Additionally, the active trapping molecule is completely removed from the carbon by elution and the stripped gold will be found in organic medium, which is incompatible with the hydrometallurgical processes that are currently installed in real on-site factories.

No effort has been done so far to develop a thiol covalently functionalized activated carbon for this application, which might represent an interesting alternative since covalent bonding is more likely to remain grafted [20] during gold adsorption processes. Additionally, covalent thiol grafting may allow the employment of greener, aqueous eluents to strip gold, avoiding the use of organic solvents and allowing the proposal of an integral, environmentally friendly process, in accordance to current hydrometallurgical on-site facilities.

Furthermore, the interaction mechanism between gold (I) thiosulfate and thiol groups covalently anchored on activated carbon and the possible Au–S structures that may be formed working under acid and basic conditions have never been studied, as far as we know. Neither is the transformation of these thiol functions after gold adsorption and elution, which could be key to propose a way of carbon reloading and recycling.

In this context, the goal of this research is to develop a covalently thiol functionalized activated carbon capable of efficiently trapping $[Au(S_2O_3)_2]^{3-}$, overcoming in that way the main obstacle that impedes its use as green leaching agent, instead of cyanide. The idea is to create a new solid enriched with thiol groups, which would augment its adsorption performance. For this purpose, a commercial coconut-based activated carbon, which is commonly used in the mining industry in Carbon-in-Pulp processes, was covalently functionalized with cysteamine as thiol carrier (functionalization process scheme shown in Fig. 1). Cysteamine was chosen as model thiol-containing molecule for two reasons: 1) it could be covalently anchored to the carbon through amide bonding and 2) it is a quite simple, linear chain molecule that contains just one thiol function, which may facilitate the understanding of the interaction between Au with S groups. Moreover, thiol functionalization was chosen due to the fact that this functional group has known affinity for Au complexes and could be easily grafted on activated carbon through covalent linking. Besides, covalent linking was preferred as functionalization approach because it is a stronger bond that is more reliable. Furthermore, this functionalization strategy permits the elution of the gold loaded carbon with green, aqueous eluents. With our study, we want to propose a modified granular activated carbon with the capacity of adsorbing Au thiosulfate and that, thanks to its characteristics, may be compatible with current Carbon-in-Pulp processes where CN^- is used as leaching agent. Our research will bring fundamental and practical knowledge that will contribute to the potential employment of thiosulfate as green leaching substance for auriferous ores that are nowadays being leached with cyanide, causing a significant environmental impact.

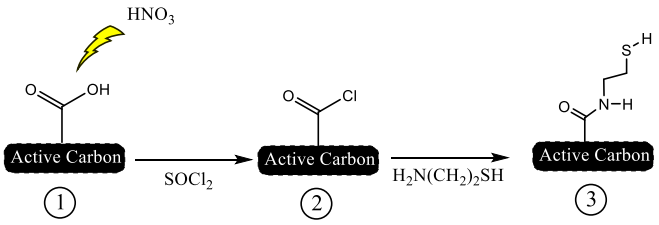


Fig. 1. Activated carbon thiol functionalization process: 1) Oxidation 2) Acylation. 3) Thiolation.

Additionally, a complete study of gold adsorption kinetics, equilibrium isotherms, influence of the solution's pH, thiol functions stability under air, changes in the carbon's texture after functionalization and green elution alternatives was carried out. Finally, the mechanism of gold thiosulfate interactions with surface sites at acid and basic conditions and the state of thiol sites after elution was unraveled by in-depth characterizations, bringing new fundamental understanding.

2. Experimental

2.1. Materials and reagents

The functionalization tests were carried out on a granular, coconut shell-based commercial activated carbon (Calgon Carbon GRC 20/22) with a particle size ranging from 1.7 to 3.4 mm. Carbon Black ENSACO® from Imerys Graphite & Carbon with a particle size of 45 μm was functionalized with thiol groups for comparison purposes. The following reagents were used: nitric acid (HNO_3, 65%, Roth), sodium hydroxide (NaOH, 99.2%, VWR), thionyl chloride ($SOCl_2$, 99.7%, Acros Organics), toluene ($C_6H_5CH_3$, 100%, VWR), cysteamine ($NH_2CH_2CH_2SH$, 96%, Sigma-Aldrich), methanol grade HPLC (100%, VWR), Argon (α1, Air liquide), gold (I) sodium thiosulfate hydrate ($Na_3Au(S_2O_3)_2 \bullet xH_2O$, 99.9%, Alfa Aesar), ammonium hydroxide solution (28.8% NH_3 basis, Sigma Aldrich), sodium chloride (NaCl, 99% Sigma-Aldrich), sodium sulfite (Na_2SO_3, 98%, Acros Organics), sodium thiosulfate anhydrous ($Na_2S_2O_3$, 99%, Alfa Aesar), potassium thiocyanate (KSCN, 98.5%, Alfa Aesar), sodium hydroxide standard solution (NaOH, 1 mol/L, Merk), sodium carbonate standard solution (Na_2CO_3, 0.05 mol/L, Merk), sodium bicarbonate ($NaHCO_3$, ≥ 99.7%, Sigma Aldrich), hydrochloric acid (HCl, 37%, VWR), potassium bromide (KBr, for spectrometric IR use, Roth), gold standard solution for atomic absorption (999 mg/L ± 4 mg/L, Sigma Aldrich), pH buffer solutions (pH 4, 7, 10, Alfa Aesar, ±0.01), deionized water.

2.2. Characterization methods and techniques

X-ray photoelectron spectroscopy (XPS) was employed to analyze the chemical environment of the samples surfaces. The analyses were carried out with a SSX 100/206 photoelectron spectrometer from Surface Science Instruments (USA) equipped with a monochromatized micro focused Al X-ray source (powered at 20 mA and 10 kV). Samples were analyzed directly in activated carbon grains form by fixating them with double-sided tape onto small brass troughs of 6 mm diameter, that were

placed on a ceramic carousel. The pressure in the analysis chamber was around 10^{-6} Pa. The angle between the surface normal and the axis of the analyzer lens was 55°. The analyzed area was approximately 1.4 mm^2 and the pass energy was set at 150 eV. In these conditions, the full width measured at half maximum (FWHM) of the Au $4f_{7/2}$ peak for a clean gold standard sample was about 1.6 eV. A flood gun set at 8 eV and a Ni grid placed 4 mm above the sample surface were used for charge stabilisation. The following sequence of spectra was recorded: survey spectrum, C 1s, O 1s, N 1s, Au $4f_{7/2}$, S $2p_3$, and C 1s again to check the stability of charge compensation with time. Data treatment was performed with the CasaXPS program (Casa Software Ltd, UK). Spectra were decomposed with the least squares fitting routine provided by the software with a Gaussian/Lorentzian (85/15) product function and after subtraction of a Shirley baseline. Molar fractions were calculated using peak areas normalized based on acquisition parameters and sensitivity factors provided by the manufacturer.

Time of flight secondary ion mass spectrometry (TOF-SIMS) was used for the chemical characterization of functionalized activated carbon samples. For this purpose, a TOF.SIMS5 instrument (IONTOF GmbH, Münster, Germany) was used. A pulsed Bi^{3+} metal ion source was employed to produce a primary beam using an acceleration voltage of 30 kV. An AC target current of 0.3 pA with a bunched pulse width lower than 1 ns was used. Both positive and negative secondary ion species were analyzed. For spectra, a raster of 128 × 128 data points over an area of 200 × 200 μm^2 was employed. The total primary ion beam dose for each analyzed area was always kept below 5×10^{11} ions.cm^{-2}, to maintain static conditions. Lateral resolution of ~3 μm and mass resolution $m/\Delta m > 5500$ at 49 *m/z* were maintained for positive and negative spectra acquisition. Under these conditions, no charge compensation was necessary. All data analyses were carried out using the software supplied by the manufacturer, SurfaceLab (version 6.5). Activated carbon grains were sticked onto Ag conductive double side adhesives and introduced directly in the chamber of the instrument for analysis.

Fourier transform infrared spectroscopy (FTIR) in transmission mode was employed to evidence the presence of functional groups in activated carbon. For this purpose, a Bruker Alpha spectrometer equipped with DTGS detector was employed. The equipment is placed inside a globe box with argon atmosphere to avoid the presence of CO_2 and water. The spectra was obtained with 100 scans in the range of 800–4000 cm^{-1} with a resolution of 2 cm^{-1}. For the analysis, KBr pellets with a dilution rate of 0.5 wt% activated carbon were prepared. The pellets' preparation involved grinding both KBr and activated carbon using a mortar and pestle until obtaining a particle size < 100 μm. Then, the KBr-carbon mixture was pressed applying 10 tons to form the pellet, which was finally dried under vacuum overnight to eliminate water interference before analysis. The spectra were exploited using OPUS software version 7.5.

Atomic Absorption Spectrometry (AAS) was employed to determine the gold concentration in solutions. This analysis was done on a PerkinElmer 3110 instrument. Calibration curves were done in the range of 2–50 ppm by direct dilution of a commercial gold standard solution.

The pH of gold thiosulfate solutions was measured with a Eutech Instruments pH510 pH-meter equipped with a SI Analytics N54 BNC probe, which was previously calibrated with buffer commercial solutions at 4, 7 and 10 pH values.

N_2-physisorption analysis was carried out with a Micromeritics equipment model ASAP 2020. Nitrogen adsorption-desorption isotherms were obtained by dosing nitrogen (77 K) in the outgassed samples (Outgassing conditions at < 5 mmHg: Evacuation phase: 90 °C, 1 h. Heating phase: 120 °C, 10 h). The equivalent specific surface area of carbon was estimated by the Brunauer-Emmett-Teller (BET) method applied in a lower P/P_0 range, as proposed by Rouquerol [25] for microporous materials. The range employed for the calculation was 0.0001–0.06. The external specific surface area was evaluated by the slope of the line drawn in the linear portion of the t-plot (calculated according to Hakins and Jura method) in the 6.5–10.3 Å thickness range. The micropore volume was given by the intercept calculated in the same range. The micropore specific surface area was estimated by the difference between the BET equivalent area and the external surface area. The distribution of pores in the material was estimated by the Density Functional Theory (DFT) method supposing a slit pores geometry.

Powdered X-ray diffraction (PXRD) was used to analyze ground activated carbon samples. The analysis was performed with a MAR345 image plate detector and an Incoatec Microfocus Source^{HIGHBRILLIANCE} (IμS^{HIGHBRILLIANCE}) Mo ELM47 operating at 50 kV and 1000 μA. The wavelength was 0.71073 Å (Mo K α radiation). The samples were filled in a 0.7 mm diameter glass capillaries and were exposed to X-rays for 15 min during which the capillary was rotated by 180°. Diffraction data was integrated by Fit2D software (using data from a 0.1 mm diameter capillary filled with LaB_6 as calibrant).

SEM imaging was done on a field-emission scanning electron microscope JEOL 7600 F operating at 15.0 kV, WD: ≈7 mm. One grain of carbon was sticked with double-phase tape on a 26 mm diameter specimen holder and was directly introduced into the analysis chamber.

TEM imaging was carried out with a LEO 922 Ω (Zeiss) Transmission Electron Microscope operating at 120 kV. Before analysis, the activated carbon samples were ground using a mortar and pestle (until attaining a particle size <100 μm) and were dispersed in ethanol. Ultrasonication was used if necessary to obtain good particles dispersion. For the analysis, one drop of the suspension was deposited on C-flat™ thick grids (Standard 20 nm Carbon, 1.2 μm hole diameter and 1.3 μm hole spacing with a 200 mesh copper grid, Protochips) and introduced directly in the analysis chamber.

Elemental analysis was used to determine the total content (% mass) of C, H, N and S in the non-functionalized and functionalized carbons. For this purpose, a FlashSmart analyzer (ThermoScientific) with TCD detector was employed. The temperature of the equipment's furnace was 950 °C and the GC column's temperature was 65 °C (packed column: length: 2 m; diameter: 6 × 5 mm). The following gases were used: helium as carrier gas (140 mL/min), helium as reference gas (100 mL/min) and oxygen (250 mL/min). The total analysis time was 720 s (oxygen injection: 5 s, sample delay: 12 s). For the analysis, 1–3 mg of ground active carbon (particle size < 100 μm) were put inside adapted crucibles and directly introduced into the analysis chamber. For S analysis, the ground carbon was put along with ≈10 mg V_2O_5 in a tin crucible.

Differentiate Boehm titrations were employed to determine activated carbon's acidity and the presence of oxygen functional groups. This characterization method for carbon materials is described in detail in the literature [26–28]. A typical experiment consisted in putting 0.5 g of activated carbon grains in contact with a solution (0.05 M) of either NaOH, Na_2CO_3 or $NaHCO_3$ for 24 h. Then, the carbon was separated by filtration and a 10 mL aliquot was taken from the filtrate. Subsequently, an exact amount of HCl solution (0.05 M) was added to acidify such aliquot (20 ml if the base was NaOH or $NaHCO_3$ and 30 mL if the base was Na_2CO_3) and this solution was degassed using Ar for at least 2 h to eliminate CO_2. Finally, the degassed solution was titrated with degassed NaOH (0.05 M) using some drops of phenolphthalein as indicator. The titration was done under Ar purging to avoid the presence of CO_2. Additionally, during the degassing and titration processes, the recipients containing the solutions were covered by a septum to avoid evaporations (see Fig. S15 in ESI).

2.3. Methods

2.3.1. Thiol covalent functionalization

Thiol functionalization of activated carbon involved the use of covalent linking techniques that, in general, include the following steps: 1) oxidation of the solid to enrich its surface with carboxylic acid groups, 2) acylation with $SOCl_2$ and 3) amide coupling with amino-thiols through the acylated carboxylic acids [18,29,30]. Concretely, in this research,

the carbon's oxidation was carried out by putting 4 g of material in contact with HNO_3 solution (2.5 M, 250 mL) for 6 h at 105 °C under reflux, using a NaOH trap for acid vapors. Afterwards, the carbon was filtrated out, washed with plenty of deionized water until obtaining a neutral pH and dried under vacuum for several hours. The oxidized activated carbon will be referred to hereinafter as ACox.

Secondly, ACox was acylated with 20 mL of thionyl chloride ($SOCl_2$) in toluene medium (130 mL) at 120 °C for 5 h, under agitation. After that, the solid was filtrated, washed with toluene (500 mL) and dried under vacuum for the night.

Thirdly, the acylated support was dispersed in 170 mL of methanol along with 1.3 equivalents of cysteamine, which were calculated according to ACox estimated total acidic functions determined by Boehm Titrations. The dispersion was mixed for 24 h at room temperature (≈20 °C) under argon atmosphere after which, it was washed with methanol (500 mL) and dried under vacuum for several hours. The thiol functionalized sample will be referred to hereinafter as AC-SH. A scheme illustrating all the functionalization steps is shown in Fig. 1 and the main reactions involved in each functionalization step are given in detail in supplementary information (Fig. S 1).

Carbon black (CB) was functionalized with thiol functions in the same way as activated carbon for comparison purposes. The functionalized carbon black will be named CB-SH.

2.3.2. Gold adsorption tests

Gold thiosulfate adsorption tests consisted of agitating 0.5 g of AC with 100 mL of gold thiosulfate solution at ambient temperature for 24 h. Then, the solid was recovered from the gold solution by filtration, dried for several hours and stored for solid characterization, while the filtrate was directly analyzed by atomic absorption to determine the remaining gold in solution after contacting with carbon. The gold thiosulfate solutions were prepared by dissolving an exact quantity of $Na_3Au(S_2O_3)_2 \bullet xH_2O$ in water to obtain different concentrations: 2 mg/L, 25 mg/L or 100 mg/L (Au basis). The solutions were analyzed before use with atomic absorption to assess their exact gold content. These working concentrations were chosen taking into consideration the typical Au content of leachates coming from real minerals extracted from Latin American countries like Ecuador, Peru and Chile, which are nowadays processed through cyanidation and Carbon-in-Pulp processes [3,31–33]. The gold loading tests were carried out at two different initial pH conditions: at ≈ pH 4, which is the unshifted pH of the solution and ≈ pH 9, which is the common pH of real Au thiosulfate solutions coming from auriferous ore leachates [9]. The solution's initial pH was adjusted by adding few drops of NH_4OH. The pH of the solution after its contact with activated carbon was measured to determine the final equilibrium pH.

The gold loaded samples used for solid characterization will be named: AC-SH.Au.pH4 or AC-SH.Au.pH9, depending on the gold loading conditions. Additionally, thiol-functionalized carbon black CB-SH was loaded with gold (0.5 g CB, 100 mL gold solution, 25 ppm initial Au concentration, pH4) under the same conditions as functionalized AC for comparison purposes. This sample will be named CB-SH.Au.

The gold adsorption efficiency (% R) was calculated according to Eq. (1), where Ci (mg/L) is the gold concentration before activated carbon contact, and Cf (mg/L) is the gold concentration after contact:

$$\% R = \frac{Ci - Cf}{Ci} * 100 \quad \text{Eq. (1)}$$

Adsorption isotherms of the functionalized activated carbon (AC-SH) were obtained to evaluate the adsorption capacity of the tested activated carbons at equilibrium, according to a methodology reported elsewhere [32,34,35]. For these tests, different masses of activated carbon (from 0.1 to 0.7 g) were put in contact with 100 ml of Au solution (100 ppm initial gold concentration, pH 4 and pH 9) for 24 h under agitation. The temperature was controlled and maintained at 25 °C during all the contact time with an oil bath. Then, the carbon was recovered by filtration and the solutions were analyzed by atomic adsorption to assess the remaining gold content in solution. The experimental data was adjusted and processed using the Freundlich isotherm model (according to Eqs. (2) and (3)) and the K-value was calculated with the isotherm data. The K-value is the activated carbon loading (in mg Au/g AC) at equilibrium when the remaining gold concentration is 1 mg Au/L. This parameter is usually used to report the gold loading capacity of activated carbons [34].

$$\frac{X}{M} = KCf^{1/n} \quad \text{Eq. (2)}$$

$$Log\frac{X}{M} = LogK + \frac{1}{n}\log Cf \quad \text{Eq. (3)}$$

In the equations, X = mass of Au adsorbed in 24 h (mg); M = mass of AC (g); Cf = remaining concentration of Au in solution at equilibrium; n and K are Freundlich constants that can be calculated with Eq. (3).

2.3.3. Elution tests

Elution tests consisted in two phases: 1) Gold loading phase: carried out according to the procedure described in point 2.3.2 above, working at 25 ppm gold concentration, pH 4. 2) Elution phase: The gold loaded carbon (herein referred to as AC-SH.Au) was contacted with 25 mL of eluent under agitation for 24 h at 50 °C. For heating, an oil bath was used along with a cold-water refrigerant to minimize evaporations. When the contact time had passed, the carbon was recovered by filtration while the solution was transferred directly to a 50 ml volumetric flask. The eluted AC was washed with water and the washings added to the filtrate until reaching the flask's graduation mark. This solution was analyzed by atomic adsorption and then the mass of gold in the eluent was calculated. The eluted solid (herein referred to as AC-SH eluted) was dried and stored for solid characterization. The elution efficiency was determined with Eq. (4) by comparing the mass of Au in the eluent and the mass of Au in the carbon before elution. For calculation details and scheme of elution process see Fig. S2.

$$\% \ elution \ efficiency = \frac{mass \ of \ Au \ in \ eluent}{mass \ of \ Au \ in \ AC \ before \ elution} * 100 \quad \text{Eq. (4)}$$

Elution solutions were prepared by dissolving an exact amount of reagents in water to obtain a desired molar concentration (M). Three elution solutions were tested: KSCN, 1 M; NaCl, 2 M + Na_2SO_3, 0.1 M and $Na_2S_2O_3$, 1 M + NH_4OH, 0.1 M.

2.3.4. Thiol functions stability under air storage

To determine the stability of thiol functions under air storage, two samples were synthetized under the same conditions, as described in section 2.3.1. The first one (AC-SH air) was stored inside a desiccator at RT, while the second one (AC-SH Ar) was stored inside a glovebox under argon atmosphere. Both samples were loaded with gold thiosulfate (25 ppm, pH 4, according to section 2.3.2) during a period of 4 months to assess their recovery capacity over time. Additionally, XPS analyses were carried out on the carbon to assess the possible thiols oxidation during this testing time under air storage.

3. Results and discussion

3.1. Activated carbon oxidation and acylation

The presence of oxygen groups in carbon materials has a direct effect on its surface chemical properties and its adsorption behavior. By oxidation, carbon acquires new characteristics like higher acidity, hydrophilicity and wettability, as well as enhanced biocompatibility and reactivity towards certain molecules [36–39]. Besides, oxygen groups like carboxylic acids, lactones and phenols, can serve as anchors for other functionalities, opening possibilities to graft a variety of heteroatoms like S and N on its surface [14,40].

Carbon can be enriched with surface oxides through different techniques. The most used one is the wet chemistry approach in which the solid is contacted with liquid oxidants such as H_2O_2, $AgNO_3$ or strong acids at different concentrations and temperatures [37,39]. In this research, HNO_3 was chosen to oxidize activated carbon, as it has been reported in the literature [15,37,39] that it could enrich the surface of the material with carboxylic acid groups, which is the desired oxygenated functionality for creating an amide coupling in further functionalization steps.

To assess the carbon's modification and presence of oxidized species after treatment, the so-obtained ACox was characterized by Differentiate Boehm Titrations, FTIR and XPS. Firstly, Boehm Titrations evidenced that the material's total acidity increased from 8 mmol/100 g AC (non-oxidized carbon) to 156 mmol acid sites/100 g AC after treatment, where 80 mmol/100 g AC corresponded to carboxylic acid groups, 33 mmol/100 g AC to lactones and 43 mmol/100 g AC to phenols.

Secondly, different oxidized functional groups were detected by FTIR. As shown in Fig. 2, ACox presents new characteristic bands compared to the non-oxidized one (Blank): a band at ≈ 1720 cm^{-1} that could be attributed to the C═O stretching of the carbonyl group in carboxylic acids, lactones and ketones [41–43], a band at ≈ 1570 cm^{-1} that has been observed by many authors in oxidized samples and has been assigned to C═C aromatic ring stretching vibration [42] or highly conjugated C═O groups [41], two sharp bands at ≈ 1384 cm^{-1} and ≈810 cm^{-1} assigned to NO_3 asymmetric stretching and NO bending vibration, respectively [43], which denotes the existence of inorganic nitrates that could be present due to HNO_3 residue in the sample. Finally, an increase of intensity of a broad band at ≈ 1100 cm^{-1} is observed which could be due to the presence of alcoholic C–O stretching of phenols and O–H bend/stretching [42,43].

Thirdly, XPS analysis done on the oxidized and non-oxidized carbons corroborated the increment of oxidized functional groups thanks to HNO_3 treatment. Table 1 shows the O 1s and C 1s XPS quantification of activated carbons before and after the oxidation process. First of all, it is noticed that the oxidized sample (ACox) contains significantly higher O content compared to the non-oxidized carbon (Blank). Indeed, while 8.6% at. of O was detected in the non-functionalized sample, the oxidized one presents 15.8% at. of this element. Furthermore, by decomposition of the C 1s peaks of both samples, it could be confirmed that the oxidation treatment causes an increment on the amount of all oxidized species linked to C (see columns O═C–O, C═O, O–C–O, C–O in Table 1). For more detail, the C 1s HR peak's decomposition of Blank and ACox are given in Fig. S3 A and B.

After its oxidation, activated carbon was acylated with $SOCl_2$ to "activate" its oxidized functions for the formation of an amide bond in the next step (see scheme in Fig. 1). XPS analysis was done on the acylated carbon to corroborate the presence of Cl in the sample. Indeed, as it could be observed in Fig. S 4, the Cl 2p3 HR XPS peak was detected in this sample at 200.4 eV, which has been assigned to Cl linked to C [44]. Additionally, it can be noticed in Table 1, that the amount of O quantified by XPS in the acylated support (AC-Cl) decreases after the acylation step, mainly due to the reduction of the amount of carboxylic acid groups (component O═C–O). This observation confirms that the expected reaction has indeed taken place, since $SOCl_2$ is supposed to react mainly with this type of oxidized species. The decomposition of the C 1s peak of AC-Cl is given in Fig. S3 C.

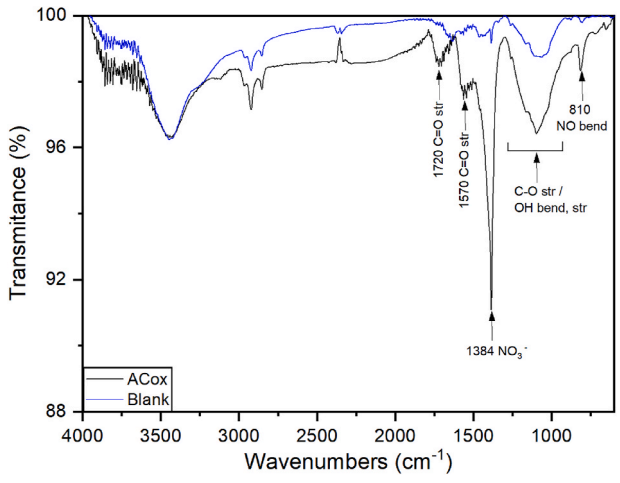


Fig. 2. FTIR of non-functionalized (Blank) and HNO_3 oxidized activated carbon (ACox). (A colour version of this figure can be viewed online.)

Table 1
XPS analysis quantification of non-functionalized and functionalized activated carbon samples. In the table: O═C–O represents groups like carboxylic acids, C═O, O–C–O corresponds to groups like ketones and ethers and C–O is assigned to groups like phenols. The C 1s peak's decomposition and components assignment have been done according to Ref. [44].

XPS analysis quantification							
Element →	O 1s	C 1s					
Sample	**Total O**	Shake-up	O=**C**–O	**C**=O, O–**C**–O	**C**–O	**C**-(C, H)	**Total C**
	Atomic percentage excluding H (% at.)						
Blank	8.6	8.6	1.5	2.7	2.0	75.2	90.0
ACox	15.8	6.0	3.4	3.6	3.4	65.3	81.7
AC-Cl	11.7	6.8	2.5	3.1	3.6	68.7	84.7

3.2. Thiolation

The presence of thiol groups on the surface of the S-functionalized carbon (named AC-SH) was corroborated by XPS, FTIR and TOF-SIMS analysis. Firstly, the AC-SH XPS survey scan (Fig. 3A) presents a new peak at ≈ 165 eV, whose biding energy corresponds to S 2p, which is not detected in the survey spectra of the non-treated AC (Blank). Additionally, the S 2p high resolution (HR) peak (Fig. 3B and D) of AC-SH allows to distinguish two sulfur components with their doublets (S $2p_{3/2}$ and S $2p_{1/2}$): a first one located at 164.0 ± 0.2 eV (S $2p_{3/2}$), that could be attributed to -C-S-(H) (thiols) [20,45] and a second component located at a higher binding energy at around 168.2 ± 0.3 eV (S $2p_{3/2}$), which may correspond to an oxidized sulfur form like sulfates (C–SO_3) [46,47]. Furthermore, as shown in Fig. 3C, AC-SH presents a new nitrogen peak located at lower biding energies compared to the Blank, where the only component detected was at ≈ 406.5 eV, attributed to an oxidized form of nitrogen like nitrates (C–NO_3) [48]. The N 1s HR peak of AC-SH was resolved in two components at ≈ 399.6 eV and 401.5 eV. The first one is assigned to the amide bond [20] between cysteamine and the carbonyl groups in the sample, which corroborates the success of the covalent functionalization process, while the second one may correspond to a protonated form of nitrogen that could be due to the presence of the zwitterionic cysteamine moiety [49,50] that is not bound covalently but physically adsorbed on the surface or/and a possible protonation of the nitrogen involved in the amide coupling due to the analysis conditions [51].

FTIR analysis (Fig. 4) verifies the presence of thiols in AC-SH. Several new peaks are detected in the functionalized sample: a weak band at 2550 cm^{-1} corresponding to S–H stretching [52,53], a band at 1580 cm^{-1} assigned to C═O stretching of amides [20] and a band at 860 cm^{-1} assigned to C-SH in-plane deformation vibration [43]. Finally, a band at 1700 cm^{-1} is seen, corresponding to C═O stretching of carboxylic acid groups [43], which is present due to the sample's prior oxidation and the fact that not all of them would react with the S-containing molecules.

By analyzing AC-SH with TOF-SIMS in positive and negative modes, several fractions of the grafted functional groups were detected, as illustrated in Fig. S 5. At $m/z \approx 33.0$, a peak attributed to $-SH^-$ fragment is observed; additionally, the whole fragment corresponding to

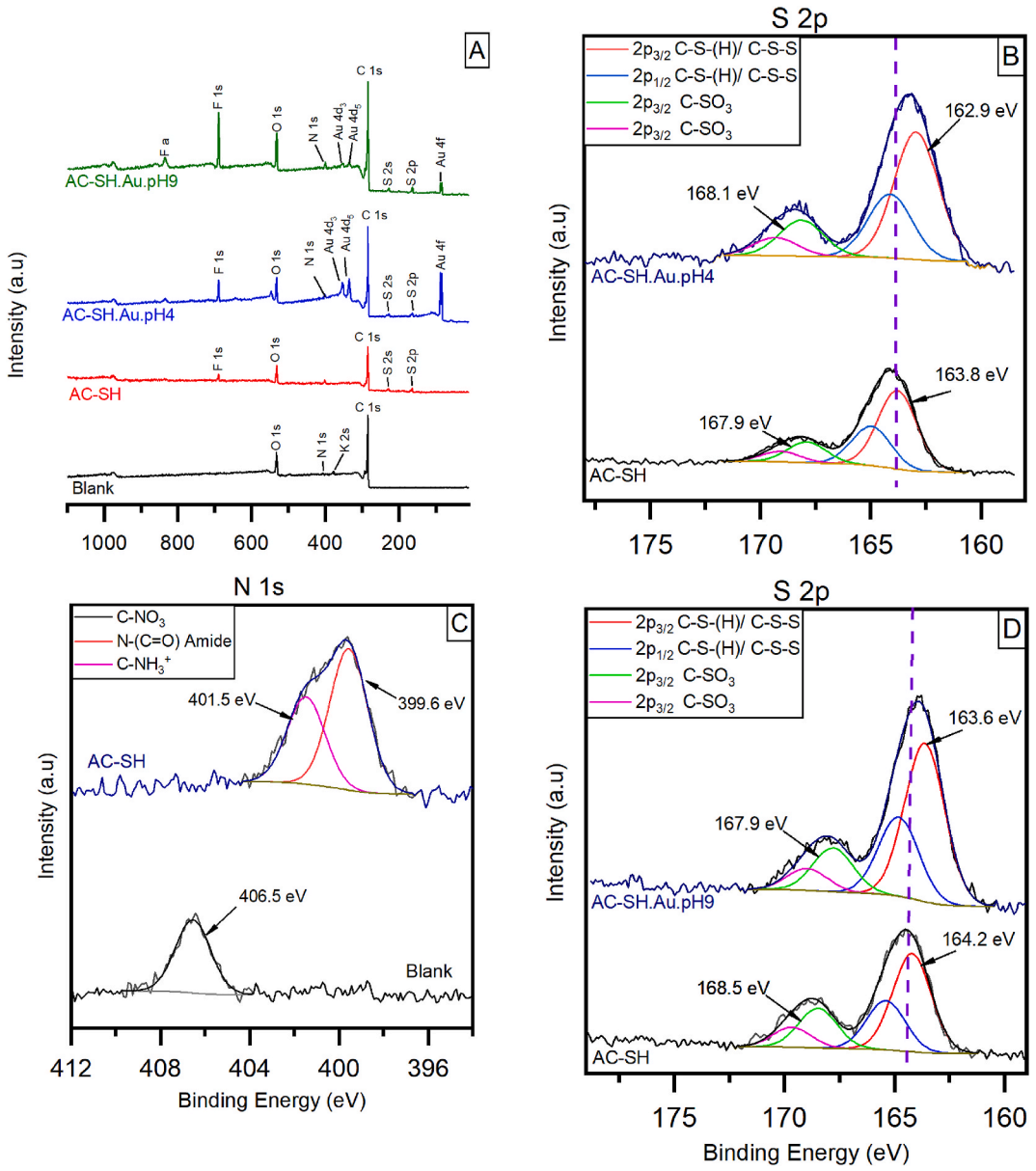


Fig. 3. XPS analysis. A) Survey spectra. B) S 2p HR peak of AC-SH and AC-SH.Au.pH4 C) N 1s HR peak of AC-SH and Blank. D) S 2p HR peak of AC-SH and AC-SH.Au.pH9. (A colour version of this figure can be viewed online.)

–NH–CH_2-CH_2-SH^- is detected at $m/z \approx 76.0$, verifying the presence of the expected functions as pending arm, grafted onto activated carbon. Furthermore, the fragment $S–S^-$ is detected at $m/z \approx 64.0$, which denotes the presence of disulfide bonds that may be formed due to the oxidation of two thiol functions located close together [54]. It is important to notice that the C–S–S species are detected at the same binding energy in XPS as thiols -C-S(H), ≈163.8 eV [44], so the contribution of this XPS peak in AC-SH may be due to the presence of both species.

Finally, through elemental analysis characterization of the non-functionalized and thiol functionalized samples (Table S3), it was determined that all the engaged S was incorporated in the solid in the last functionalization step, since the amount of S detected in the thiol functionalized sample (AC-SH) is really close to the amount of S added to react with the acylated support (see calculation details in Fig. S 17 in ESI). Considering that no S was quantified in the non-functionalized activated carbon, all the S detected in AC-SH may come from cysteamine and therefore, it can be concluded that a quantitative reaction yield has been attained. Nevertheless, we may suppose that there could also be a contribution of some non-bounded cysteamine that may have stayed physically trapped within the porous network of carbon.

3.2.1. *Changes in the carbon's surface area and texture due to the functionalization process*

Changes in the carbon's surface area and texture before and after functionalization treatments have been assessed through physisorption analysis and SEM imaging. As it can be seen in Table 2, the non-functionalized material (Blank) presents an elevated specific surface area (1066 m^2/g) due to a well-developed microporosity (microporous surface area: 1061 m^2/g). After oxidation, the total specific surface area of the carbon (ACox) is reduced to 927 m^2/g, with a drop in the microporous volume and microporous surface area (919 m^2/g), while the external surface area seems to increase slightly after treatment. Regarding AC-SH, a significant reduction of the total surface area of the material after functionalization is evidenced, with a clear impact on the microporous surface area, which was reduced from 1061 m^2/g (Blank) to 490 m^2/g. The external surface area of AC-SH seems unchanged. These three samples present a Type I adsorption isotherm (Fig. S6) with a H4 hysteresis type, typical of activated carbons, which corroborates

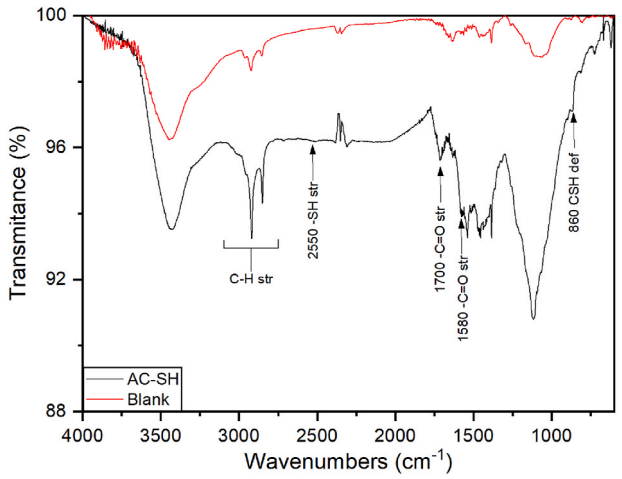


Fig. 4. FTIR spectra of non-functionalized (Blank) and thiolated (AC-SH) activted carbons.

Table 2
Physisorption analysis of non-functionalized (Blank) and functionalized activated carbons: ACox and AC-SH. The Standard deviations shown in this table have been calculated between samples of the same type, synthetized and measured at different moments.

Sample	BET equivalent specific surface area (m^2/g)	Microporous surface area (m^2/g)	Microporous volume (cm^3/g)	External surface area (m^2/g)
Blank	1066 ± 43	1061 ± 42	0.42 ± 0.02	5 ± 1
ACox	927 ± 20	919 ± 18	0.36 ± 0.01	8 ± 1
AC-SH	496 ± 15	490 ± 14	0.20 ± 0.01	6 ± 1

the microporosity character of the materials [55].

Moreover, the pores' distribution estimated by DFT (Fig. 5) reveals that the Blank has a maximum pores width of 20 Å, with a notable region of pores between 13.6 Å to 18.6 Å. Then, when the carbon is oxidized (ACox), the maximum pores' width increases to 30 Å and a new region of pores within the region 17 Å to 30 Å is created. Regarding the thiolated carbon (AC-SH), the maximum pores width is 30 Å and a region of pores between 13.6 Å to 30 Å is observed.

The changes in the material's texture due to the functionalization processes could be explained by several reasons including the production of humin substances as by-product that could block the carbon's micropores [16], the harsh conditions that could cause the micropores walls to collapse [56,57], leading to a reduction of the microporous volume, and finally a possible pore blockage by the created functional groups [16].

Additionally, SEM imaging (Fig. S7) reveals a notable change in the carbon's texture through the different functionalization steps. For instance, big pores of around 1 μm could be identified after the carbon's oxidation (ACox), that are still present in the sample after the contact with cysteamine (AC-SH), which may explain the increase of external surface area evidenced by physisorption analysis. Also, it can be observed that the thiolation process (AC-SH) has a "cleaning" effect on the carbon's surface, since it seems smoother than after oxidation, and it creates wide open grooves in the material.

3.3. Gold adsorption tests

Fig. 6 illustrates the gold recovery performances at 2, 25 and 100 ppm of the non-functionalized (Blank) and thiolated (AC- SH) samples, working at acid and basic pH. It is evident that the presence of thiols on the carbon surface enhances its ability to adsorb $[Au(S_2O_3)_2]^{3-}$, with an uptake of up to 100% at 2 and 25 ppm gold concentration (pH 4), compared to low recovery performances of the non-functionalized sample under these conditions (16% recovery at 2 ppm and 8% recovery at 25 ppm). When working at basic pH, the AC-SH gold adsorption performance remains unchanged at 2 and 25 ppm initial gold concentrations, while the Blank increases its uptake to 18 and 20%, respectively. Furthermore, when working at a higher gold concentration (100 ppm), the functionalized carbon traps up to ≈ 70% of gold from the solution at pH 4 and the behavior of the sample remains similar at basic pH, while the Blank increases its gold uptake up to 32% under these conditions. For additional information, Table S1 in ESI shows the equilibrium pHs measured after the gold solutions were contacted with the tested activated carbons.

Besides, by analyzing the kinetics data shown in Fig. 7 A, it was determined that AC-SH adsorbs all the gold from the solution in 8 h contact time (corresponding to 50 mg Au/g AC) at pH 4 and its behavior is similar working at pH 9. Additionally, the Au adsorption rate of the functionalized carbon, which was calculated by determining the slope of the kinetics curve from 0 to 8 h (Fig. 7 B), is found to be 5.43 mg Au/g AC*h when the adsorption is done at acid pH and 5.68 mg Au/g AC h for basic conditions. Since in real Carbon-in-Pulp facilities for AuCN recovery, activated carbon is usually in contact with the mineral pulp for a total contact time of 8–12 h [3,58], the adsorption time of our

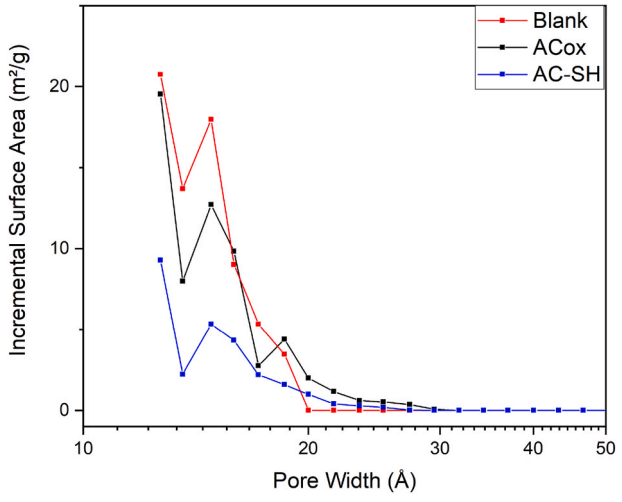


Fig. 5. DFT pores distribution of non-functionalized (Blank) and functionalized activated carbons. (A colour version of this figure can be viewed online.)

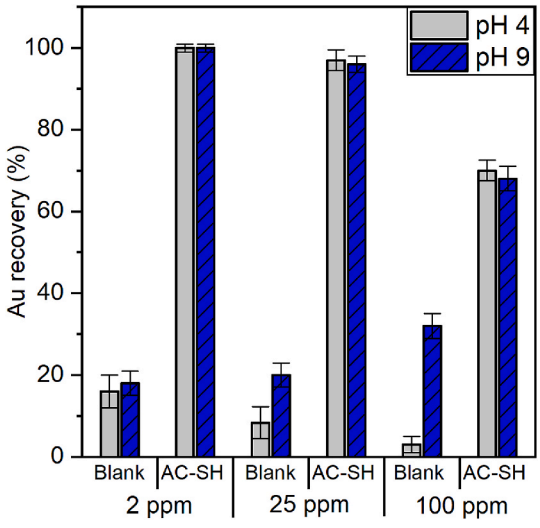


Fig. 6. Non-functionalized (Blank) and thiolated (AC-SH) activated carbons gold recovery performances at pH 4 and pH 9.

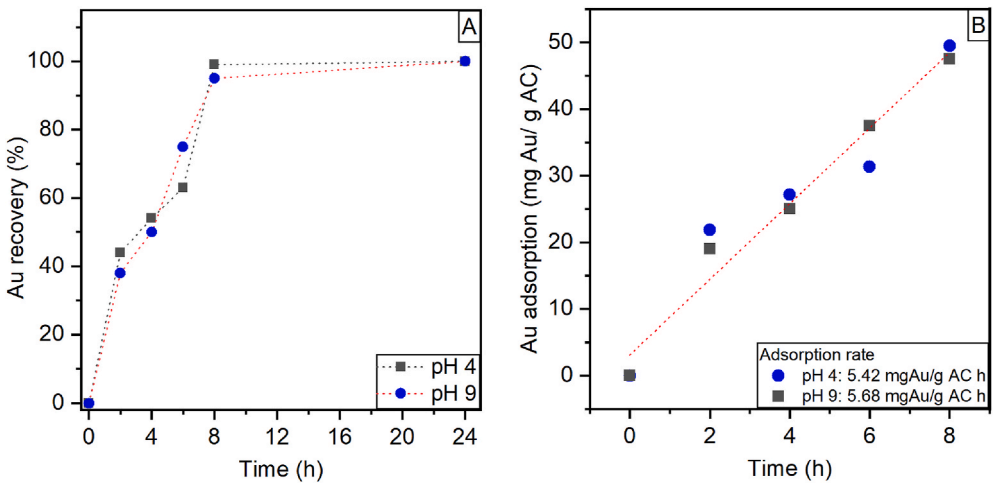


Fig. 7. A) AC-SH gold adsorption kinetics in 24 h. B) AC-SH gold adsorption rate between 0 and 8 h. Conditions: 25 ppm, 100 mL, 0.5 g AC, pH 4 and 9.

functionalized carbon may not constitute a limitation for its actual application in current installed processes. Moreover, if we compare the performance of other developed S-functionalized carbons applied in Au thiosulfate adsorption (ref. [23,24]) where the adsorption equilibrium in similar testing conditions was reached upon 24–50 h contact, it could be considered that, for this application, our thiol functionalized activated carbon constitutes a performance asset.

Fig. 8 shows the equilibrium gold adsorption isotherms of the thiol functionalized activated carbon AC-SH at pH 4 and pH 9. The carbon samples were contacted with the Au solution for 24 h to ensure that Au adsorption equilibrium has been reached. As it could be observed, a good fitting of the experimental data was obtained with the Freundlich model, as could be confirmed with the reported R^2 values [32,34,35]. From the isotherm data fitting, the K-value parameter at a residual Au

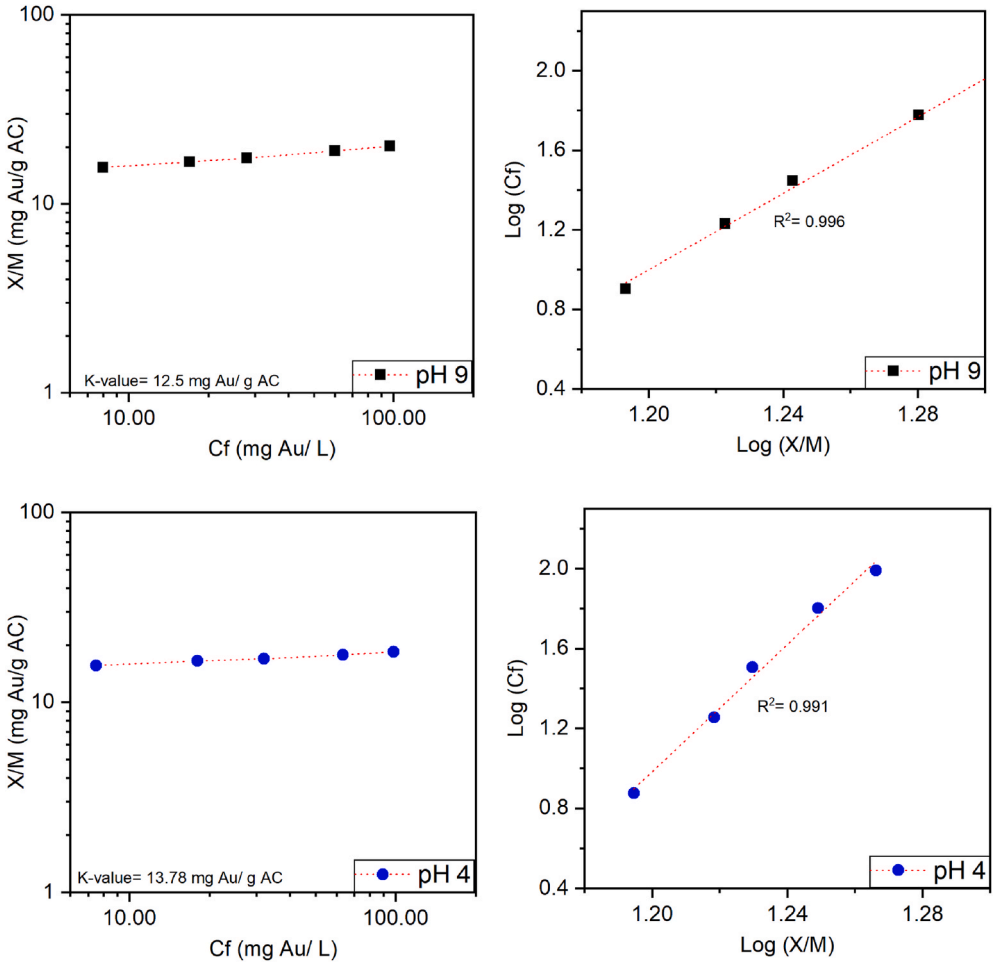


Fig. 8. Equilibrium gold adsorption isotherms on thiol -functionalized activated carbon AC-SH. Conditions: 100 ppm initial Au concentration, 100 mL, 24 h, pH 4 or pH 9, 25 °C.

concentration of 1 mg/L was calculated. The K-value, which is used to estimate the gold adsorption capacity of activated carbons [34] was found to be 13.78 mg Au/g AC when the adsorption was carried out at acid pH, and 12.5 mg Au/g AC, when the adsorption was done under basic conditions. The calculated Freundlich constants are given in Table S2 in ESI.

XPS analysis done on the gold loaded sample under acid conditions (AC-SH.Au.pH4) corroborates the presence of gold on the carbon's surface and its link with –SH functions. Firstly, the survey spectrum of this sample (Fig. 3A) presents several peaks that could be assigned to Au, with the main one located at ≈ 84 eV, corresponding to Au 4f. The Au 4f HR peak (Fig. S 8A) reveals that the Au 4 $f_{7/2}$ component is located at 84.4 eV, which could be attributed to Au in oxidation state +1 [59]. The XPS surface atomic quantification reveals that the ratio Au/C–S(H) is around 1.5.

Secondly, regarding the S 2p HR peak of AC-SH.Au.pH4 (Fig. 3B), we observe a shift of around 0.9 eV towards lower binding energies in the C–S-(H) component after gold loading, from 163.8 eV (AC-SH) to 162.9 eV (AC-SH.Au.pH4). This shift proves the existence of a strong interaction between Au and –SH, as it has been reported that unbound thiols appear at a binding energy around 163.8–164.2 eV, while when thiols interact with Au, the thiol peak moves towards lower energies [45]. In general, a XPS peak shift towards lower binding energies denotes an increase of the negative charge density of the involved atom. More interestingly, it has been demonstrated that there is a direct correlation between this S 2p shift and the theoretical charge density of sulfur from thiols, when it is linked with gold monolayers [60]. Indeed, it has been stated that the sulfur atom involved in this interaction becomes more negatively charged when forming the Au–S bound. This shift has been interpreted by other authors as the formation of the Au-thiolate bond [61].

TOF-SIMS analysis of AC-SH.Au.pH4 confirms and complements the information obtained by XPS. Fig. S9 shows the most relevant fragments detected in the negative ion spectra of this sample. First, at $m/z \approx 229.0$, the species $Au–S^-$ is observed, which corroborates the formation of a covalent bond between Au and S, as seen by XPS. More interestingly, other fragments attributed to Au–S interactions are discovered at $m/z \approx$ 426.0, 654.9 and 883.8. These species could be attributed to Au_2S^-, $Au_3S_2^-$ and $Au_4S_3^-$ fragments, respectively. This denotes that the interaction between Au and S is not limited to a one to one connection (e.g., one thiol function could form a covalent bond with just one Au thiosulfate complex), but that they are capable of forming Au–S "chains", where even 4 Au atoms could be linked to 3 S atoms ($Au_4S_3^-$). This explains why the Au/C–S(H) ratio detected by XPS is > 1. Finally, at $m/z \approx 111.93$, the species $S_2O_3^{2-}$ could be seen only in the negative ion mode, which may denote that after the formation of the Au (I) – S bond, $S_2O_3^{2-}$ stays as counter-ion of Au^{1+}.

Regarding the thiolated carbon that was gold loaded under basic conditions (AC-SH.Au.pH9), the XPS survey spectrum reveals several gold peaks including the one at 84 eV, attributed to Au 4f (Fig. 3A), comparable to the case of AC-SH.Au.pH4. Furthermore, the S 2p HR XPS peak (Fig. 3D) evidences a similar shift (≈0.6 eV) of the C–S(H) component towards lower binding energies after gold contact, which confirms the formation of a Au-thiolate bond, as explained before at acid conditions. We remark, however, that the Au 4 $f_{7/2}$ component (Fig. S 8B) is located at slightly lower binding energies (84.2 eV) in this sample (AC-SH.Au.pH4: 84.4 eV), which may reveal the presence of other Au species. To corroborate this hypothesis, complementary PXRD analysis was carried out with the gold loaded samples, as it has been reported in the literature that carbon materials might have a reductive character [62], being capable of reducing Au^{1+} species to Au^0 [63]. Fig. 9 shows the diffraction spectra of the gold loaded samples under acid and basic conditions. As it could be seen, all the samples loaded at basic pH (Fig. 9B) show 5 small peaks located at $2\Theta \approx 17°$, 20°, 28°, 33° and 34° whose positions and intensities fit well with the Au^0 simulated spectra reflections (COD ID 1100138 [64]), confirming the presence of this species. In contrast, when the gold loading is done under acid conditions (Fig. 9A), no Au^0 reflections are detected, and only 3 featureless broad humps at $2\Theta \approx 11°$, 20° and 34° are seen. These humps correspond to the (002), (100) and (111) reflections of graphite, as it is known that activated carbons contain small ordered sp^2 regions [65], and they are observed in all the analyzed samples. This phenomena could be explained by the fact that when Au is involved in a basic medium, rich in OH^-, it could be transformed into Au(OH) which precipitates on the surface, and then, the latter could be reduced to Au^0 by the electron-rich carbon surface. This is not the case in acidic conditions, where no Au (OH) could be formed [66]. Moreover, the presence of Au^0 species may explain why the non-functionalized carbon (Blank.Au.pH9) increases its Au uptake under basic conditions.

TEM imaging has been used as a complementary analytical technique to verify the presence and size of Au^0 species in AC-SH.Au.pH9. As it could be observed in Fig. S 10, Au nanoparticles of around 10 nm are indeed found in this gold loaded sample.

Concerning TOF-SIMS analysis done on AC-SH.Au.pH9 (Fig. S9), similar Au–S fragments are found including: AuS^- ($m/z \approx 229.0$), Au_2S^- ($m/z \approx 426.0$), $Au_3S_2^-$ ($m/z \approx 654.9$) and $Au_4S_3^-$ ($m/z \approx 883.8$). Finally,

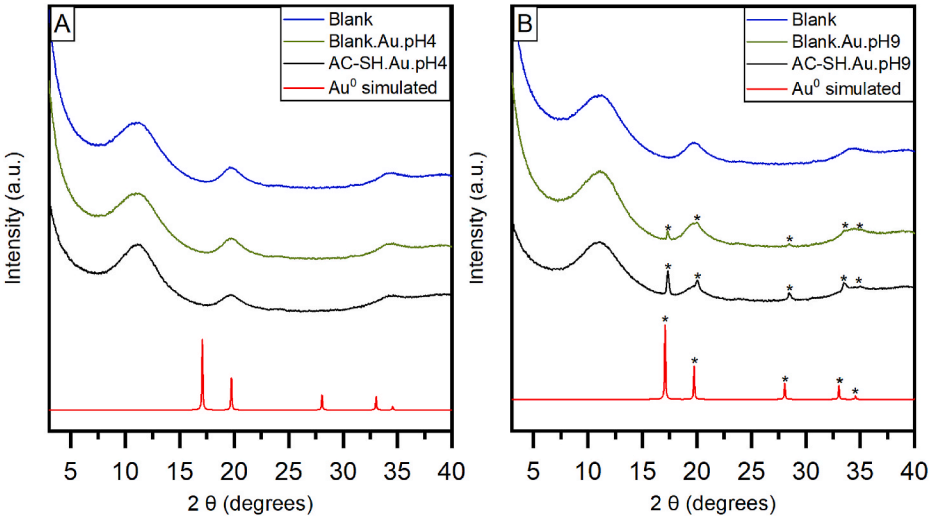


Fig. 9. PXRD analysis of non-functionalized carbon (Blank) and gold loaded samples (100 ppm) at: A) acid conditions and B) basic conditions. (A colour version of this figure can be viewed online.)

$S_2O_3^{2-}$ ($m/z \approx 111.93$) could be seen again just in the negative ion mode, corroborating the presence of this anion as charge-balancing species.

Finally, aiming to understand if the interactions between Au and S groups occur in the outer-layers of AC or if its highly-developed microporosity plays an important role in Au thiosulfate adsorption, carbon black was functionalized and then gold loaded under the same conditions as AC. It is important to remark that CB possesses a considerably smaller specific surface area (≈68 m^2/g) due to absence of micropores, compared to activated carbon. Therefore, if having a high specific surface area was important for gold adsorption, this material is expected to show a poorer performance than AC. Interestingly, it was found that while the non-functionalized CB could trap just 3% of Au from the solution, the functionalized one achieved 100% gold recovery (25 ppm initial Au concentration, 100 ml, 0.5 g CB), showing the same performance as the functionalized activated carbon AC-SH, under these conditions. This may mean that the interactions between Au thiosulfate and thiol groups occur in the most external layers of the functionalized activated carbon and that the reduction of specific surface area that faces the solid due to the functionalization procedures does not affect its adsorption capacity. The S 2p and Au 4f XPS HR peaks of the thiol functionalized (CB-SH) and gold loaded (AC-SH.Au) carbon blacks are given in ESI in Fig. S11.

With all this information at hand and based on known Au (I) thiolate structures previously reported in the literature [67], we propose 2 different adsorption mechanisms for the gold loaded samples under acid and basic conditions, as illustrated in Fig. 10. At acid conditions, several gold-thiolate interactions may occur including: 1 Au^{1+} atom linked to S, 2 Au^{1+} atoms connected to one S function or a thiol bridge where 3 or even 4 Au^{1+} atoms connected to 2 or 3 S functions are plausible, in agreement with the Au/S surface ratio detected by XPS and confirmed structures observed by TOF-SIMS. At basic conditions, the same Au–S interactions occur but, additionally, Au^0 nanoparticles are as well present (as verified by TEM imaging and XRD analysis).

The S– Au bonds may be formed according to the following main reaction, which has been previously reported in the literature when studying thiol-gold adsorption systems [68,69]:

$$Au^{1+} + R\text{–}SH \rightarrow R\text{–}S^{-}\text{-}\ Au^{1+} + \tfrac{1}{2}\ H_2$$

Regarding the Au^0 nanoparticles that are observed on the activated carbon surface when the adsorption is carried out under basic conditions, they may be formed according to the following reactions [66]:

$$Au^{1+} + OH^{-} \rightarrow Au(OH)$$

$$2\ Au(OH) + e^{-} \rightarrow 2\ Au^0 + H_2O + \tfrac{1}{2}\ O_2$$

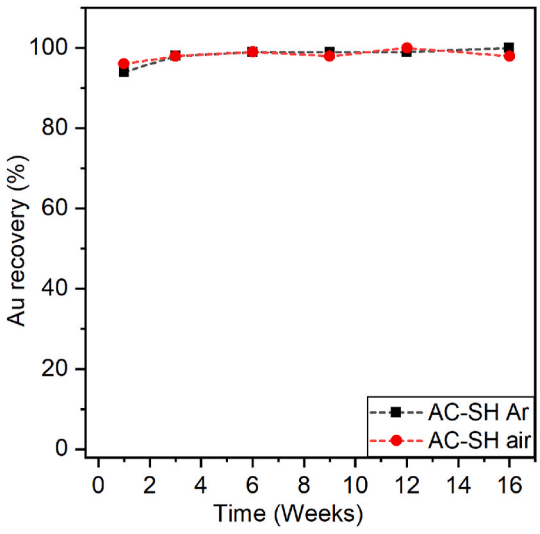


Fig. 11. Gold loading performance of thiol functionalized carbon during 16 weeks under air or argon storage. Gold loading conditions: 25 ppm, 100 mL, 24 h, 0.5 g AC, pH 4.

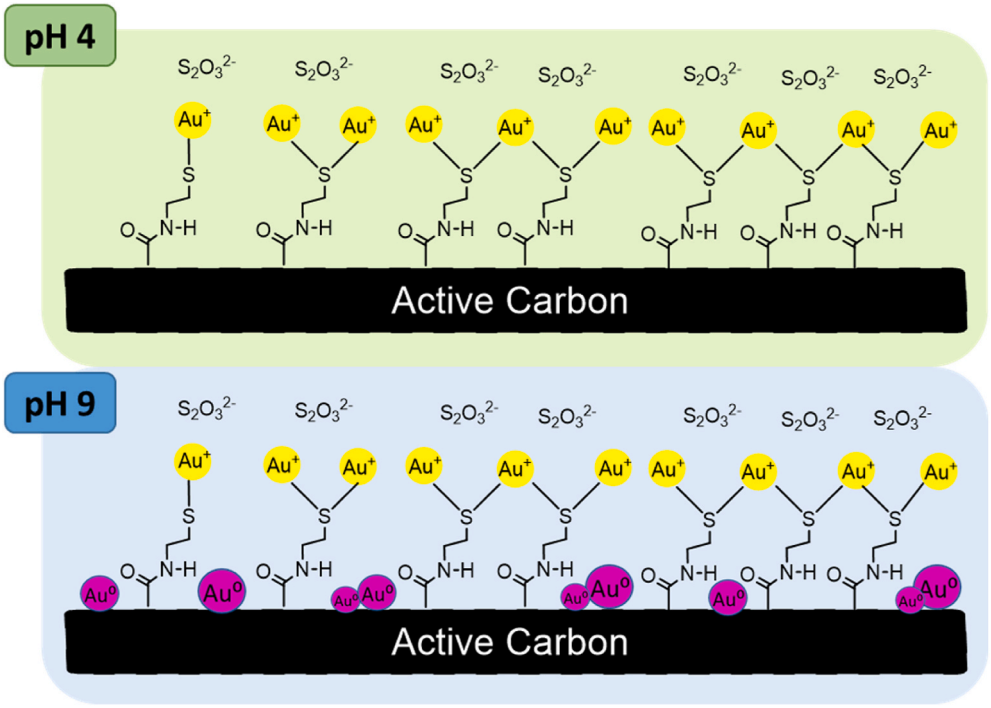


Fig. 10. Schemes representing the possible Au thiosulfate adsorption mechanism in thiol functionalized carbon and its formed structures under acid and basic conditions.

3.4. Stability of thiol functions under air

Figs. 11 and 12 show the results of the stability tests done on AC-SH under air and argon storage for 16 weeks. Firstly, in Fig. 11, it could be noticed that the gold adsorption performance of the air-stored sample is similar to the one stored under argon during 16 weeks, having a maximum gold recovery throughout all this time. Additionally, the S 2p HR XPS peak (Fig. 12) of the air-stored sample shows that the content of the oxidized sulfur components changes only slightly during this time: from 18 % at. (week 1) to 21 % at. (week 16). Therefore, it could be said that thiol functions are stable under air storage conditions for at least 16 weeks and most importantly, their gold adsorption performance remains unaffected even with the possibility of air oxidation.

3.5. Elution tests

Once AC-SH has been successfully loaded with gold, it is time to consider the stripping stage. For this purpose, several eluents that are commonly used for resins elution [70], have been tested. As shown in Table 3, the best elution results are obtained working with $Na_2S_2O_3$ + NH_4OH solution, where up to 71% of gold could be stripped from the carbon.

Furthermore, these elution tests give deeper fundamental information on the kind of interactions occurring between gold and sulfur functions. In ion-exchange resins, since gold thiosulfate is adsorbed by reversible ion-exchange phenomena, gold stripping can be carried out by ionic molecules that will displace Au thiosulfate, taking its place as counter-ion [12]. However, in the present case, the bond between gold and sulfur sites is stronger than electrostatic interactions due to the formation of Au thiolate, whose strength is known to be close to the Au–Au bond [67]. Therefore, the stripping of Au from carbon is difficult using ionic molecules like NaCl + Na_2SO_3 and KSCN, which in contrast, show good performances in resins' elution.

Since $Na_2S_2O_3$ + NH_4OH solution was found to be the best eluent, further solid characterization was carried out just with this sample. As shown in Fig. 13A, the XPS S 2p HR peak of the carbon after elution (AC-SH eluted) reveals two sulfur components, one at 163.7 eV (S 2 $p_{3/2}$) and a second at 168.2 eV (S 2 $p_{3/2}$). The peaks' position in this sample is similar to the one found in the thiol functionalized sample (AC-SH). Moreover, it is observed that after elution, the shift towards lower binding of the C–S(H) component found in the gold loaded sample (AC-SH.Au) is no longer present, in other words, this component moved from 162.9 eV to 163.7 eV, which may indicate that the bound between Au and S was broken. It is important to notice that the S species detected in AC-SH eluted seem not to come from $Na_2S_2O_3$ residue on the solid's surface, since the S 2p HR peak of pure powdered $Na_2S_2O_3$ (Fig. 13B) looks notably different, with its S 2 $p_{3/2}$ components at 161.9 eV and 167.9 eV. Additionally, in Fig. 13A, it could be observed that the S 2 $p_{3/2}$ peak at 168.2 eV attributed to oxidized sulfur species in the AC-SH eluted sample has increased from ≈18% (AC-SH) to 35% (AC-SH eluted). This is expected since the eluted sample has been contacted with aqueous solutions twice, and therefore, more sulfur species could have been oxidized.

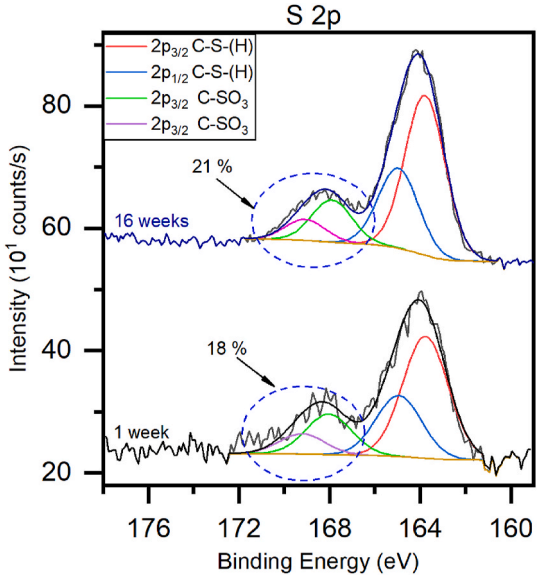


Fig. 12. XPS S 2p HR peak of thiol functionalized carbon after 1 and 16 weeks under air storage. (A colour version of this figure can be viewed online.)

Table 3
Elution efficiency results with different eluents. Elution carried out with 25 mL of eluent at 50 °C for 24 h.

Eluent, molar concentrations	Elution efficiency
KSCN, 1 M	1%
NaCl, 2 M + Na_2SO_3, 0.1 M	2%
$Na_2S_2O_3$, 1 M + NH_4OH, 0.1 M	71%

Table 4 shows the S and Au XPS quantification results of AC-SH, AC-SH.Au and AC-SH eluted. Firstly, it is observed that the amount of Au detected in the eluted sample (0.1% at.) is remarkably smaller than the one detected in the gold loaded one (4.3% at.). Similar results are seen by TOF-SIMS, where the fractions $Au–S^-$, Au_2S^-, $Au_3S_2^-$ and $Au_4S_3^-$ appear in significantly less normalized intensity in the eluted sample, compared to the same normalized peaks in the Au loaded one (Fig. S 12). These results demonstrate the successful stripping of Au from the carbon, in corroboration to XPS observations. Additionally, as shown in Table 4, it is noticed that after elution, the total sulfur amount quantified by XPS (Total S) decreases from 5.0% (AC-SH) to 1.7% (AC-SH eluted), which means that not only Au is stripped from the solid, but also some sulfur functions are lost in this process. However, with TOF-SIMS analysis done on AC-SH eluted, –SH and S–S fragments (m/z ≈ 33.0 and 64.0, respectively) are still detected, though in smaller normalized intensity compared to AC-SH (Fig. S 13 and Fig. S 14).

Similarly to what happens when resins are used in gold thiosulfate systems, it seems that the eluted carbon needs to be enriched with active thiol functions before being used again in a new gold loading process. This regeneration could consist in functionalizing it again with a thiol-containing molecule, or more interestingly, we could take advantage of the S–S bridges that are still present in the sample (as verified by XPS and TOF-SIMS) and transform them into active thiols by a reduction processes. For this purpose, some tests inspired by procedures applied to polysulfide-containing rubber materials where dithiothreitol is used as reducing agent [71] have been done, and promising results have been obtained.

4. Conclusions

Granular activated carbon has been successfully functionalized with thiol functions through covalent bonds. This functionalized carbon has been characterized and tested with gold thiosulfate solution and a remarkable enhancing of the gold adsorption performance after treatment has been proven working under acid and basic conditions and different Au concentrations. Kinetics studies reveal that AC-SH traps all the gold from the solution working at 25 ppm Au concentration in 8 h contact time and that the pH of the solution has little influence on the gold adsorption performance of the thiolated sample. The K-value of the functionalized carbon was determined by equilibrium gold adsorption isotherms: at acid conditions, it corresponds to 13.78 mg Au/g AC, while under basic conditions, it is estimated at 12.5 mg Au/g AC. The thiol-functionalized sample seems stable under air storage for at least 16 weeks. Functionalization processes provoke a reduction of the solid's specific surface area and microporous volume, though comparative tests

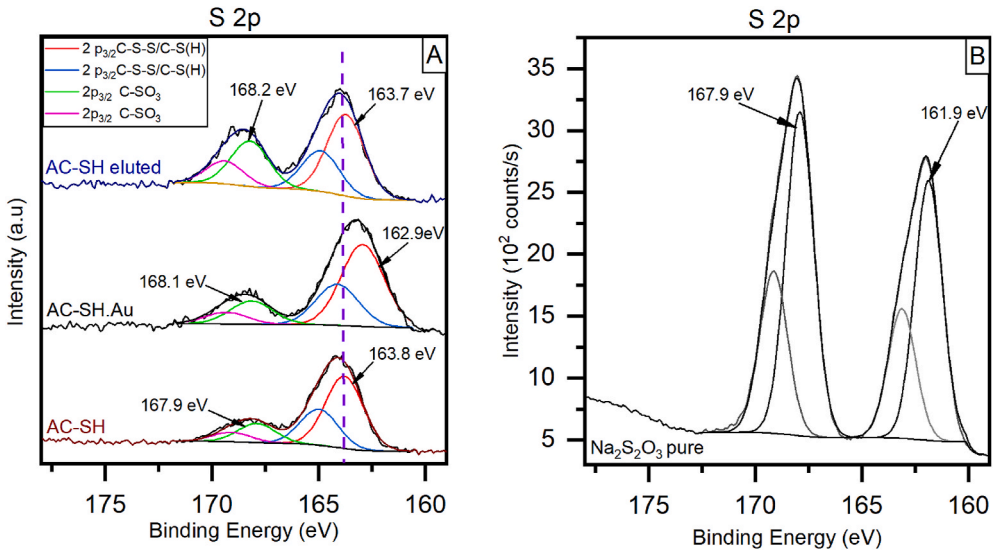


Fig. 13. S 2p HR XPS peak of: A) Thiol-functionalized carbon (AC-SH), Gold loaded carbon (AC-SH.Au) and carbon eluted with $Na_2S_2O_3$ + NH_4OH solution (AC-SH eluted). B) Sodium thiosulfate pure reagent. (A colour version of this figure can be viewed online.)

Table 4
S and Au XPS quantification of AC-SH, AC-SH.Au and AC-SH eluted samples. The quantification is expressed in atomic percentage excluding H (% at.). BE denotes the species' binding energy in eV.

Sample	SOx		C–S(H)/C–S–S/C–S–Au		Total S	Total Au
	% at.	BE: (eV)	% at.	BE: (eV)	% at.	% at.
AC-SH	0.9	167.9	4.1	163.8	5.0	–
AC-SH.Au	1.0	168.1	3.6	162.9	4.6	4.3
AC-SH eluted	0.6	168.2	1.1	163.7	1.7	0.1

with carbon black suggest that Au interactions with S functions occur in the most outer-layers of activated carbon, hence, the reduction of surface area does not affect the Au adsorption capacity of the functionalized solid. In-depth solid characterization have demonstrated that the gold adsorption mechanism on the functionalized activated carbon depends on the pH of the solution: at acid pH, the formation of a Au^{1+}-S chains has been evidenced, which allows the adsorption of high amounts of gold, since the Au–S bonding is not limited to a one to one Au–S interaction. At basic pH, in addition to the same Au^{1+}-S chains, Au^0 species are observed. Stripping of the gold loaded sample has been accomplished at up to 71% level using $Na_2S_2O_3$ and NH_4OH as eluent. Our proposal brings a new perspective that would contribute to open doors to greener gold-mining processes. S-functionalized activated carbon may permit to extend the use of non-pollutant leaching agents like thiosulfate, while being in accordance with the current hydrometallurgical on-site facilities. In future works, it would be interesting to compare this S-functionalized activated carbon with carbons functionalized with other heteroatoms like N, for instance in the form of amine groups, to establish differences in important aspects like performances and adsorption or elution mechanisms.

CRediT authorship contribution statement

Nathalie de la Torre-Miranda: Writing – original draft, Conceptualization, Methodology, Investigation, Formal analysis, Visualization, Writing – review & editing. **Laoise Reilly:** Investigation, Formal analysis. **Pierre Eloy:** Data curation, Formal analysis. **Claude Poleunis:** Data curation, Formal analysis. **Sophie Hermans:** Conceptualization, Supervision, Resources, Project administration, Funding acquisition, Writing – review & editing.

Declaration of competing interest

The authors declare that they have no known competing financial interests or personal relationships that could have appeared to influence the work reported in this paper.

Acknowledgements

The authors are thankful to Conseil d'Action International (CAI) and ARES scholarship programs for funding this research. We thank Jean François Statsyns for his constant technical support and help. We are grateful to Departamento de Metalurgia Extractiva (DEMEX) from Escuela Politécnica Nacional in Quito, Ecuador, for supplying the non-functionalized granular Calgon carbon and for the constant technical cooperation between our institutions. We thank Timothy Steenhaut for his invaluable help in PXRD analysis, Fabien Drault for his support in TEM imaging, Delphine Magnin for her help in SEM analysis and Fabio Lucaccioni for carrying out elemental analysis.

Appendix A. Supplementary data

Supplementary data to this article can be found online at https://doi.org/10.1016/j.carbon.2022.12.061.

References

[1] GoldHub, World, Gold council, gold mine prod. https://www.gold.org/goldhub/data/historical-mine-production, 2021. (Accessed 5 May 2020).
[2] S. Giovanni, Convening Actors to Reduce Child Labour and Improve Working Conditions in Artisanal and Small-Scale Gold Mining (Caring Gold Project): Fact Sheet, Ghana, 2019 https://www.ilo.org/manila/publications/WCMS_720740/lang–en/index.htm.
[3] P.C. Velásquez-López, M.M. Veiga, B. Klein, J.A. Shandro, K. Hall, Cyanidation of mercury-rich tailings in artisanal and small-scale gold mining: identifying strategies to manage environmental risks in Southern Ecuador, J. Clean. Prod. 19 (2011) 1125–1133, https://doi.org/10.1016/j.jclepro.2010.09.008.
[4] M.M. Veiga, D. Nunes, B. Klein, J.A. Shandro, P.C. Velasquez, R.N. Sousa, Mill leaching: a viable substitute for mercury amalgamation in the artisanal gold mining sector? J. Clean. Prod. 17 (2009) 1373–1381, https://doi.org/10.1016/j.jclepro.2009.03.012.
[5] G. Hilson, S. Pardie, Mercury: an agent of poverty in Ghana's small-scale gold-mining sector? Resour. Pol. 31 (2006) 106–116, https://doi.org/10.1016/j.resourpol.2006.09.001.
[6] G. Chi, M.C. Fuerstenau, J.O. Marsden, Study of Merrill-Crowe processing. Part I: solubility of zinc in alkaline cyanide solution, Int. J. Miner. Process. 49 (1997) 171–183.

[7] W.P. Staunton, Carbon-in-Pulp, gold ore process, 535–552, https://doi.org/10.1016/B978-0-444-63658-4.00030-X, 2016.
[8] R. Schnepp, Cyanide: sources, perceptions, and risks, J. Emerg. Nurs. 32 (2006) 3–7, https://doi.org/10.1016/j.jen.2006.05.008.
[9] M.G. Aylmore, D.M. Muir, Thiosulfate leaching of gold-a review, miner, Eng. Times 14 (2001) 135–174, https://doi.org/10.1016/S0892-6875(00)00172-2.
[10] B. Xu, W. Kong, Q. Li, Y. Yang, T. Jiang, X. Liu, A review of thiosulfate leaching of gold: focus on thiosulfate consumption and gold recovery from pregnant solution, Metals 7 (2017), https://doi.org/10.3390/met7060222.
[11] C. Abbruzzese, P. Fornari, R. Massidda, F. Vegliò, S. Ubaldini, Thiosulphate leaching for gold hydrometallurgy, Hydrometallurgy 39 (1995) 265–276, https://doi.org/10.1016/0304-386X(95)00035-F.
[12] Z. Dong, T. Jiang, B. Xu, Y. Yang, Q. Li, Recovery of gold from pregnant thiosulfate solutions by the resin adsorption technique, Metals 7 (2017) 95–111, https://doi.org/10.3390/met7120555.
[13] H. Zhang, I.M. Ritchie, S.R. La Brooy, The adsorption of gold thiourea complex onto activated carbon, Hydrometallurgy 72 (2004) 291–301, https://doi.org/10.1016/S0304-386X(03)00182-8.
[14] Chung Deborah, Carbon Materials. Science and Applications 3, Engineering Materials for Technological Needs, New York, 2019.
[15] C.Y. Yin, M.K. Aroua, W.M.A.W. Daud, Review of modifications of activated carbon for enhancing contaminant uptakes from aqueous solutions, Sep. Purif, Technol. 52 (2007) 403–415, https://doi.org/10.1016/j.seppur.2006.06.009.
[16] P. Chingombe, B. Saha, R.J. Wakeman, Surface modification and characterisation of a coal-based activated carbon, Carbon N. Y. 43 (2005) 3132–3143, https://doi.org/10.1016/j.carbon.2005.06.021.
[17] B. Roop, G. Meenakshi, Activated Carbon Adsorption, Ilustrada, CRC Press, 2005.
[18] R. Zanella, E.V. Basiuk, P. Santiago, V.A. Basiuk, E. Mireles, I. Puente-Lee, J. M. Saniger, Deposition of gold nanoparticles onto thiol-functionalized multiwalled carbon nanotubes, J. Phys. Chem. B 109 (2005) 16290–16295, https://doi.org/10.1021/jp0521454.
[19] J. Gooding, Alkanethiol self-assembled monolayers, in: H.S. Nalwa (Ed.), Encycl. Nanosci. Nanotechnol, American Scientific Publishers, California, 2004, pp. 17–49. http://fulviofrisone.com/attachments/article/462/ENN-Vol 1.pdf.
[20] P. Gobbo, M.C. Biesinger, M.S. Workentin, Facile synthesis of gold nanoparticle (AuNP)–carbon nanotube (CNT) hybrids through an interfacial Michael addition reaction, Chem. Commun. 49 (2013) 2831–2833, https://doi.org/10.1039/c3cc00050h.
[21] T. Nishino, T. Ito, Y. Umezawa, Carbon nanotube scanning tunneling microscopy tips for chemically selective imaging, Anal. Chem. 74 (2002) 4275–4278, https://doi.org/10.1021/ac020215m.
[22] Z. Liu, Z. Shen, T. Zhu, S. Hou, L. Ying, Z. Shi, Z. Gu, Organizing single-walled carbon nanotubes on gold using a wet chemical self-assembling technique, Langmuir 16 (2000) 3569–3573, https://doi.org/10.1021/la9914110.
[23] Y. Chen, F. Zi, X. Hu, P. Yang, Y. Ma, H. Cheng, Q. Wang, X. Qin, Y. Liu, S. Chen, C. Wang, The use of new modified activated carbon in thiosulfate solution: a green gold recovery technology, Sep. Purif, Technol. 230 (2020), https://doi.org/10.1016/j.seppur.2019.115834.
[24] Y. Chen, F. Zi, X. Hu, H. Yu, Y. Nie, P. Yang, H. Cheng, Q. Wang, X. Qin, S. Chen, Y. Zhang, Grafting of organic sulfur-containing functional groups on activated carbon for gold(I) adsorption from thiosulfate solution, Hydrometallurgy 185 (2019) 102–110, https://doi.org/10.1016/j.hydromet.2019.02.007.
[25] J. Rouquerol, P. Llewellyn, F. Rouquerol, Is the BET Equation Applicable to Microporous Adsorbents? in: J. R, N.S.P.L. Llewellyn, F. Rodriquez-Reinoso (Eds.), Stud. Surf. Sci. Catal. Elsevier B.V., 2007, pp. 49–56.
[26] H.P. Boehm, Chemical identification of surface groups, adv, Catalyst 16 (1966) 179–274, https://doi.org/10.1016/S0360-0564(08)60354-5.
[27] A.C. Tarasuk, H.A. Andreas, A.M. Oickle, S.L. Goertzen, K.D. Thériault, Standardization of the Boehm titration. Part I. CO2 expulsion and endpoint determination, Carbon N. Y. 48 (2009) 1252–1261, https://doi.org/10.1016/j.carbon.2009.11.050.
[28] Y.O. Abdalla, A.M. Oickle, H.A. Andreas, K.R. Hopper, S.L. Goertzen, Standardization of the Boehm titration: Part II. Method of agitation, effect of filtering and dilute titrant, Carbon N. Y. 48 (2010) 3313–3322, https://doi.org/10.1016/j.carbon.2010.05.004.
[29] V. Basiuk, E. Basiuk, Chemical derivatization of carbon nanotube tips, in: H. S. Nalwa (Ed.), Encycl. Nanosci. Nanotechnol, American Scientific Publishers, California, 2004, pp. 761–776.
[30] D. Vidick, A.F. Leonard, C. Poleunis, A. Delcorte, M. Devillers, S. Hermans, Phosphine- and ammonium-functionalized ordered mesoporous carbons as supports for cluster-derived metal nanoparticles, Catal. Today 235 (2014) 112–126, https://doi.org/10.1016/j.cattod.2014.03.017.
[31] C. Cacciuttolo, D. Cano, Environmental impact assessment of mine tailings spill considering metallurgical processes of gold and copper mining: case studies in the andean countries of Chile and Peru, Water 14 (2022) 3057, https://doi.org/10.3390/w14193057.
[32] R.B. Cevallos Toledo, C.F. Aragón-Tobar, S. Gámez, E. de la Torre, Reactivation process of activated carbons: effect on the mechanical and adsorptive properties, Molecules 25 (2020), https://doi.org/10.3390/molecules25071681.
[33] R.R. Jannas, R.E. Beane, B.A. Ahler, D.R. Brosnahan, Gold and copper mineralization at the El Indio deposit, Chile, J. Geochem. Explor. 36 (1990) 233–266, https://doi.org/10.1016/0375-6742(90)90057-H.
[34] J.O. Marsden, C. lain House, The Chemistry of Gold Extraction, second ed., Society for Mining, Metallurgy and Exploration, Inc, Colorado, USA, 2006.
[35] A. Shipman, J. Jativa, Mintek Manual on Testing of Activated Carbons, 1987. Johannesburg, South Africa.
[36] S.S. Barton, M.J.B. Evans, E. Halliop, J.A.F. MacDonald, Acidic and basic sites on the surface of porous carbon, Carbon N. Y. 35 (1997) 1361–1366, https://doi.org/10.1016/S0008-6223(97)00080-8.
[37] C. Moreno-Castilla, M.V. López-Ramón, F. Carrasco-Marín, Changes in surface chemistry of activated carbons by wet oxidation, Carbon N. Y. 38 (2000) 1995–2001, https://doi.org/10.1016/S0008-6223(00)00048-8.
[38] J. Boudou, J. Paredes, A. Cuesta, A. Martinez- Alonso, J. Tascón, Oxygen plasma modification of pitch-based isotropic carbon fibres, Carbon N. Y. 41 (2003) 41–56.
[39] H.P. Boehm, Surface oxides on carbon and their analysis: a critical assessment, N. Y, Carbon 40 (2002) 145–149, https://doi.org/10.1016/S0008-6223(01)00165-8.
[40] N. Karousis, N. Tagmatarchis, D. Tasis, Current progress on the chemical modification of carbon nanotubes, Chem. Rev. 110 (2010) 5366–5397, https://doi.org/10.1021/cr100018g.
[41] C. Moreno-Castilla, M.A. Ferro-García, J.P. Joly, I. Bautista-Toledo, F. Carrasco-Marín, J. Rivera-Utrilla, Activated carbon surface modifications by nitric acid, hydrogen peroxide, and ammonium peroxydisulfate treatmenss, Langmuir 11 (1995) 4386–4392, https://doi.org/10.1021/la00011a035.
[42] S. Shin, J. Jang, S.H. Yoon, I. Mochida, A study on the effect of heat treatment on functional groups of pitch based activated carbon fiber using FTIR, N. Y, Carbon 35 (1997) 1739–1743, https://doi.org/10.1016/S0008-6223(97)00132-2.
[43] G. Socrates, Infrared and Raman Characteristic Group Frequencies, third ed., John Wiley & Sons Ltd., England, 2001.
[44] NIST X-ray Photoelectron Spectroscopy Database, NIST Standard Reference Database Number 20, National Institute of Standards and Technology, Gaithersburg MD, 20899 (2000), doi:10.18434/T4T88K, (retrieved [december, 2022]).
[45] C.J. Zhong, R.C. Brush, J. Anderegg, M.D. Porter, Organosulfur monolayers at gold surfaces: reexamination of the case for sulfide adsorption and implications to the formation of monolayers from thiols and disulfides, Langmuir 15 (1999) 518–525, https://doi.org/10.1021/la980901+.
[46] M. Fantauzzi, B. Elsener, D. Atzei, A. Rigoldi, A. Rossi, Exploiting XPS for the identification of sulfides and polysulfides, RSC Adv. 5 (2015) 75953–75963, https://doi.org/10.1039/c5ra14915k.
[47] M. Descostes, F. Mercier, N. Thromat, C. Beaucaire, M. Gautier-Soyer, Use of XPS in the determination of chemical environment and oxidation state of iron and sulfur samples: constitution of a data basis in binding energies for Fe and S reference compounds and applications to the evidence of surface species of an oxidized py, Appl. Surf. Sci. 165 (2000) 288–302, https://doi.org/10.1016/S0169-4332(00)00443-8.
[48] S. Aduru, S. Contarini, J.W. Rabalais, Electron-, X-ray-, and ion-stimulated decomposition, J. Phys. Chem. 90 (1986) 1683–1688.
[49] A. Cossaro, M. Dell'Angela, A. Verdini, M. Puppin, G. Kladnik, M. Coreno, M. De Simone, A. Kivimäki, D. Cvetko, M. Canepa, L. Floreano, Amine functionalization of gold surfaces: ultra high vacuum deposition of cysteamine on Au(111), J. Phys. Chem. C 114 (2010) 15011–15014, https://doi.org/10.1021/jp104824c.
[50] H. Fleischer, Y. Dienes, B. Mathiasch, V. Schmitt, D. Schollmeyer, Cysteamine and its homoleptic complexes with group 12 metal ions. Differences in the coordination chemistry of ZnII, CdII, and HgII with a small N,S-donor ligand, Inorg. Chem. 44 (2005) 8087–8096, https://doi.org/10.1021/ic050814m.
[51] J.S. Stevens, S.J. Byard, C.A. Muryn, S.L.M. Schroeder, Identification of protonation state by XPS, solid-state NMR, and DFT: characterization of the nature of a new theophylline complex by experimental and computational methods, J. Phys. Chem. B 114 (2010) 13961–13969, https://doi.org/10.1021/jp106465u.
[52] Z. Xia, L. Baird, N. Zimmerman, M. Yeager, Heavy metal ion removal by thiol functionalized aluminum oxide hydroxide nanowhiskers, Appl. Surf. Sci. 416 (2017) 565–573, https://doi.org/10.1016/j.apsusc.2017.04.095.
[53] R. Nagarjuna, M.S.M. Saifullah, R. Ganesan, Oxygen insensitive thiol-ene photo-click chemistry for direct imprint lithography of oxides, RSC Adv. 8 (2018) 11403–11411, https://doi.org/10.1039/c8ra01688g.
[54] N. Spiliopoulou, C.G. Kokotos, Photochemical metal-free aerobic oxidation of thiols to disulfides, Green Chem. 23 (2021) 546–551, https://doi.org/10.1039/d0gc03818k.
[55] K.S.W. Sing, R.T. Williams, Physisorption hysteresis loops and the characterization of nanoporous materials, Adsorpt. Sci. Technol. 22 (2004) 773–782, https://doi.org/10.1260/0263617053499032.
[56] T. Xu, X. Liu, Peanut shell activated carbon: characterization, surface modification and adsorption of Pb2+ from aqueous solution, Chin. J. Chem. Eng. 16 (2008) 401–406, https://doi.org/10.1016/S1004-9541(08)60096-8.
[57] G.-F. Zhao, P. Bai, H.-M. Zhu, R.-X. Yan, X.-M. Liu, Zi-Feng Yan, the modification of activated carbons and the pore structure effect on enrichment of coal-bed methane, Asia-Pacific J, Chem. Eng. 3 (2008) 284–291, https://doi.org/10.1002/apj.147.
[58] W. Stange, The process design of gold leaching and carbon-in-pulp circuits, J. South African Inst. Min. Metall (1999) 13–26. January/F.
[59] A. McNeillie, D.H. Brown, W.E. Smith, M. Gibson, L. Watson, X-ray photoelectron spectra of some gold compounds, J. Chem. Soc., Dalton Trans. (1980) 767–770, https://doi.org/10.1039/DT9800000767.
[60] B. Lindberg, K. Hamrin, G. Johansson, U. Gelius, A. Fahlman, C. Nordling, K. Siegbahn, Molecular Spectroscopy by Means of ESCA II. Sulfur compounds. Correlation of electron binding energy with structure, Phys. Scripta 1 (1970) 286–298.
[61] D.G. Castner, K. Hinds, D.W. Grainger, X-ray photoelectron spectroscopy sulfur 2p study of organic thiol and bisulfide binding interactions with gold surfaces, Langmuir 12 (1996) 5083–5086, https://doi.org/10.1021/la960465w.
[62] H. Yang, X. Cui, X. Dai, Y. Deng, F. Shi, Carbon-catalysed reductive hydrogen atom transfer reactions, Nat. Commun. 6 (2015) 1–11, https://doi.org/10.1038/ncomms7478.

[63] G. Bond, C. Louis, D. Thompson, Catalysis by Gold, sixth ed., Imperial College Press, London, 2006.
[64] A. Vaitkus, A. Merkys, S. Gražulis, Validation of the crystallography open database using the crystallographic information framework, J. Appl. Crystallogr. 54 (2021), https://doi.org/10.1107/S1600576720016532.
[65] A. Lazzarini, A. Piovano, R. Pellegrini, G. Agostini, S. Rudić, C. Lamberti, E. Groppo, Graphitization of activated carbons: a molecular-level investigation by INS, DRIFT, XRD and Raman techniques, Phys. Procedia 85 (2016) 20–26, https://doi.org/10.1016/j.phpro.2016.11.076.
[66] S. Hermans, A. Deffernez, M. Devillers, Preparation of Au-Pd/C catalysts by adsorption of metallic species in aqueous phase for selective oxidation, Catal. Today 157 (2010) 77–82, https://doi.org/10.1016/j.cattod.2010.04.010.
[67] H. Häkkinen, The gold-sulfur interface at the nanoscale, Nat. Chem. 4 (2012) 443–455, https://doi.org/10.1038/nchem.1352.
[68] J.R. Reimers, M.J. Ford, A. Halder, J. Ulstrup, N.S. Hush, Gold surfaces and nanoparticles are protected by Au(0)-thiyl species and are destroyed when Au(I)-thiolates form, Proc. Natl. Acad. Sci. U, S. A 113 (2016) E1424–E1433, https://doi.org/10.1073/pnas.1600472113.
[69] Q. Chi, M.J. Ford, A. Halder, N.S. Hush, J.R. Reimers, J. Ulstrup, Sulfur ligand mediated electrochemistry of gold surfaces and nanoparticles: what, how, and why, Curr. Opin. Electrochem 1 (2017) 7–15, https://doi.org/10.1016/j.coelec.2016.12.004.
[70] H. Arima, T. Fujita, W.T. Yen, Gold recovery from nickel catalyzed ammonium thiosulfate solution by strongly basic anion exchange resin, Mater. Trans. 44 (2003) 2099–2107, https://doi.org/10.2320/matertrans.44.2099.
[71] K.B. Buhl, A.H. Agergaard, R.K. Møller, M. Kongsfelt, S. Heide-Jørgensen, M. K. Budzik, M. Hinge, S.U. Pedersen, K. Daasbjerg, Facile access to disulfide/thiol containing poly(glycidyl methacrylate) brushes as potential rubber adhesive layers, ACS Appl. Polym. Mater 2 (2020) 2380–2388, https://doi.org/10.1021/acsapm.0c00306.